phys. stat. sol. (a) **204**, No. 12, 4004–4008 (2007) / **DOI** 10.1002/pssa.200777135

Magneto-transport studies of single ferromagnetic nanowire

Y. Rheem[1,2], **B.-Y. Yoo**[1,2], **W. P. Beyermann**[2,3], and **N. V. Myung**[1,2,*]

[1] Department of Chemical and Environmental Engineering, University of California-Riverside, Riverside, CA 92521, USA
[2] Center for Nanoscale Science and Engineering, University of California-Riverside, Riverside, CA 92521, USA
[3] Department of Physics and Astronomy, University of California-Riverside, Riverside, CA 92521, USA

Received 10 May 2007, revised 5 October 2007, accepted 27 October 2007
Published online 10 December 2007

PACS 75.47.-m, 75.50.Bb, 75.50.Dd, 75.50.Tt

The magnetotransport properites of individual ferromagnetic nanowires (e.g. Ni, $Co_{23}Ni_{77}$, $Ni_{85}Fe_{15}$) with 200 nm diameters were investigated. The ferromagnetic nanowires were successfully electrodeposited within an anodized alumina by controlling solution composition, temperature, and current density. Using a magnetic assembly technique, single nanowire was successfully bridged across microfabricated gold e-lecrodes. The temperature coefficient of resistance for ferromagnetic nanowires was lower than the bulk because of a larger residual resistance from increased electrical scattering in one-dimensional structures. The ferromagnetic nanowires showed typical anisotropic magnetoresistance where the magnetoresistance ratio was lower than bulk values.

1 Introduction

Recently, the electro- and magneto-transport properties of one-dimensional nanostructures including nanowires have been investigated for possible applications in high density magnetic recording and nano-scale spintronics. Despite the potential impact of the field, it remains relatively undeveloped, necessitating a more intimate understanding of spin-polarized transport properties in nanowires [1]. Limited works were reported on spin-polarized (magneto) transport across nanostructures, which were hindered by difficulties with small sample volumes and connecting to individual nanostructures. In order to bypass these obstacles, most magnetotransport studies were performed on bundles of nanowires embedded in a template [2–4]. Although averaged magnetotransport properties of nanowires can be readily obtained from this approach, it is difficult to acquire spin transport properties of an individual nanowire because of the interference from dipolar interactions between neighboring nanowires. These interactions reduced the coercivity and squareness observed in hysteresis graphs for nanowires, and changed the magnetization reversal mode from curling to coherent rotation [5, 6]. In order to measure the spin-transport of an individual nanowire without these distortions, electron-beam lithographically patterned ferromagnetic rectangular nanowires have been investigated [7]. Even though these lithographic techniques allow investigations of the magnetotransport properties of single quasi-one-dimensional nanostructure, it is difficult to control the properties, shape and dimensions of the nanowires.

In our previous studies [8–10], we reported a facile and cost-effective technique for creating a functional ferromagnetic device with a single high aspect ratio cylindrical nanowire incorporating good electrical contacts and the potential for hierarchical structures. Using this technique, temperature and diame-

* Corresponding author: e-mail: myung@engr.ucr.edu, Phone: +1 951 827 7710, Fax: +1 951 827 5696

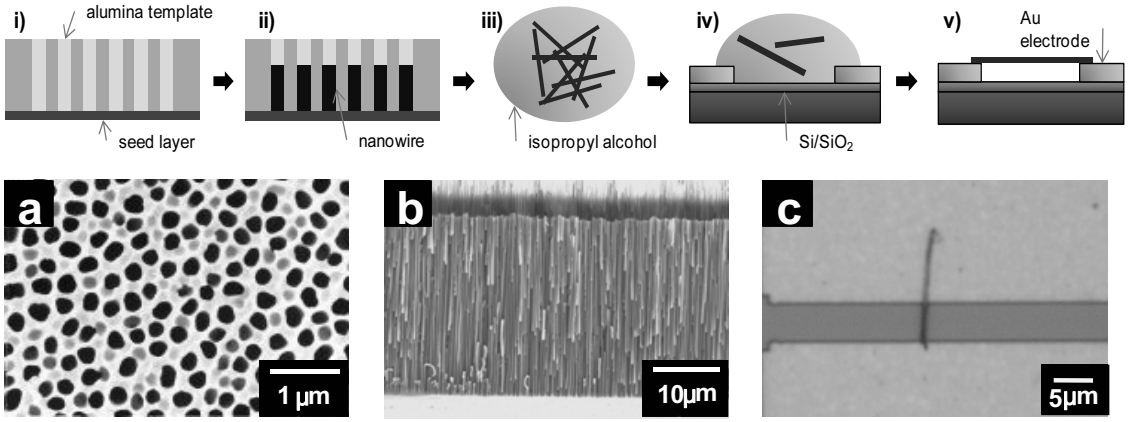

Fig. 1 Schematics of fabrication process of single nanowire assemblage on electrodes (i-v) and image of alumina nanotemplate (a), cross-section of nanotemplate with electrodeposited nanowires (b) and single nanowire interconnect on prepatterned electrodes (c).

ter dependent magnetotransport and magnetization reversal properties of single Ni, $Co_{23}Ni_{77}$ and $Ni_{85}Fe_{15}$ nanowires were investigated [11–13]. In this work, we demonstrate the manipulation and positioning of a single electrodeposited ferromagnetic nanowire on pre-patterned electrodes. In addition, we summarize the temperature dependent electro- and magneto-transport properties of ferromagnetic nanowires.

2 Experimental

Ferromagnetic nanowires were fabricated by a template directed electrodeposition method. Schematics of the fabrication steps to synthesize nanowires are shown in Fig. 1. Commercially available (Anodisc® form Whatman Inc., 200 nm normal pore size) alumina nanotemplates were used as scaffolds for nanowire electrodeposition (Fig. 1(a)). The process begins by sputtering a seed layer of approximately 200 nm of Au on one side of the nanotemplate with an Emitech K550 table-top sputter (Fig. 1(i)). Table 1 gives the electrolyte composition for single component (Ni) and alloy ($Co_{23}Ni_{77}$, $Ni_{85}Fe_{15}$) ferromagnetic nanowires. NaCl and $CaCl_2$ were used as a supporting electrolyte to enhance current efficiency, and sodium saccharin was added to reduce the deposit stress. L'ascorbic acid was used to minimize Fe^{2+} oxidation in the electrolyte [14]. The ferromagnetic nanowires were deposited using a potentiostat (EG&G PAR VMP2 multi-channel potentio/galvanostat) with a controlled current density (Fig. 1(ii) and (b)). Electrolyte pH was adjusted with either HCl or NaOH. An insoluble platinum-coated titanium strip and the saturated calomel electrode (SCE) were used as the anode and reference electrode, respectively. The length of the nanowires was controlled by adjusting the deposition time.

Table 1 Electrodeposition conditions for iron-group metal and alloy nanowires and their properties.

Composition	Electrolyte	pH	Temp. (°C)	Current Density (mA/cm^2)	Preferred Orientation	Average Grain Size (nm)	AMR (300 K)
Ni	1.28 M $Ni(H_2NSO_3)_2$ + 0.19 M $NiCl_2$ + 0.36 M H_3BO_3	4	25	10	-	30	1.9 %
$Co_{23}Ni_{77}$	0.2 M $NiCl_2$ + 0.025 M $CoCl_2$ + 0.7 M NaCl + 0.4 M H_3BO_3 + 0.0075 M sodium saccharin	3	25	10	[111]	15	3.8 %
$Ni_{85}Fe_{15}$	0.9 M $FeCl_2$ + 0.6 M $NiCl_2$ + 1.0 M $CaCl_2$ + 0.03 M L'ascorbic acid	0.3	40	5	[220]	11	2.0 %

The crystal structure of the nanowires embedded in the alumina nanotemplate was determined by X-ray diffraction with a D8 Advance Diffractometer from Bruker using Cu K_α radiation. The average grain size was determined using Debye-Scherrer's equation. After electrodeposition, the seed layer was mechanically polished, and the nanowires were released by dissolving the alumina nanotemplate in a 5 M NaOH solution for 3 days at 50 °C. After removal of the nanotemplate, the nanowires were washed with distilled water and suspended in isopropyl alcohol (Fig. 1(iii)). The nanowires were observed using scanning electron microscopy (SEM, Phillips XL30 FEG) and the composition of electrodeposited nanowires was measured by energy dispersive x-ray analysis (EDX).

Magnetic field assisted assembly was used to position a single nanowire across microfabricated Au electrodes with a 5 μm gap. After placing the prepatterned Au electrodes in an external magnetic field (~350 G), one drop of the nanowire suspension was dispensed on top of electrodes (Fig. 1(iv)). The ferromagnetic nanowires aligned along the external magnetic field direction and settled down on the electrodes (Fig. 1(v)). In order to minimize the contact resistance between the nanowire and electrode, the assembled nanowires were annealed in a reducing environment of 5 % H_2 + 95 % N_2 at 350 °C for 1 hour. The magnetoresistance was measured using a physical property measurement system from Quantum Design as function of temperature from 10 K to 300 K. The applied external magnetic field was scanned between ±10 kOe, both in the longitudinal and transverse directions relative to the nanowire axis. The voltage across the nanowire was measured with a fixed applied current of 100 μA.

3 Results and discussion

The composition of alloy nanowires along the axis was examined by selected area EDX analysis. The variation of composition along the nanowire axis was controlled within 5 at. %. The crystalline structure of the electrodeposited ferromagnetic nanowires embedded in the alumina nanotemplate was measured by X-ray diffraction. Figure 2 shows the X-ray diffraction patterns of Ni, $Co_{23}Ni_{77}$, and $Ni_{85}Fe_{15}$ nanowires. As expected, the nanowires have a face centered cubic structure. The $Co_{23}Ni_{77}$ and $Ni_{85}Fe_{15}$ nanowires have the preferred orientation along [111] and [220], respectively, whereas the Ni nanowires are randomly orientated. The average grain size was determined to be 30, 15 and 11 nm for Ni, $Co_{23}Ni_{77}$ and $Ni_{85}Fe_{15}$, respectively, which indicates the deposited ferromagnetic nanowires were nanocrystalline. For measuring the transport properties of ferromagnetic nanowires, the nanowires were assembled on photolithographically patterned gold electrodes with a 5 μm gap using an externally applied magnetic field. After magnetic alignment, the assembled nanowire were annealed in a reducing environment (5 % H_2 + 95 % N_2) to minimize the electrical contact resistance from the surface oxide and/or hydroxide formation during the template removal process. Before the annealing, the electrical contact was not established, whereas after annealing the resistance was 18, 35 and 51 Ω at 300 K for Ni, $Co_{23}Ni_{77}$ and

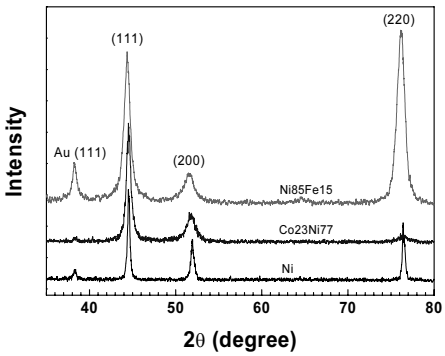

Fig. 2 X-ray diffraction patterns of electrodeposited ferromagnetic nanowires.

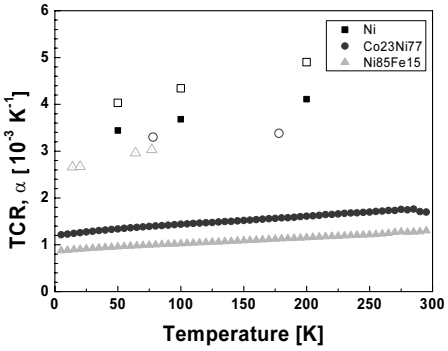

Fig. 3 Temperature coefficient of resistance of ferromagnetic nanowires and bulk counterpart (solid; nanowire, open; bulk).

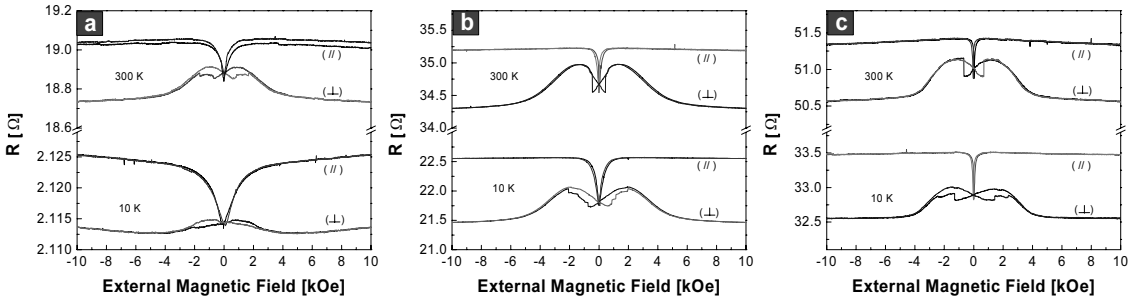

Fig. 4 Magnetoresistance profiles of single ferromagnetic (a) Ni, (b) $Co_{23}Ni_{77}$, and (c) $Ni_{85}Fe_{15}$ nanowires at 300 K and 10 K with longitudinal (//) and transverse (⊥) directions.

$Ni_{85}Fe_{15}$ nanowires, respectively. The temperature dependent resistance of the nanowires was measured with a constant current of 100 μA in the absence of an external magnetic field. As the temperature was decreased, the resistance decreased linearly. For a more detailed analysis, the temperature coefficient of resistance (TCR) was calculated using;

$$\alpha = \frac{1}{R_0}\frac{dR}{dT} \tag{1}$$

where T is the temperature, R is the electrical resistance and R_0 is the resistance at 300 K. Figure 3 shows the comparison of the TCR for electrodeposited nanowires with their bulk counterparts [15]. The TCR of the nanowires was much smaller than the bulk values and almost independent of temperature. In metals, the electrical resistivity depends on the scattering rates of the conduction electrons with phonons and lattice imperfections. The electrical resistivity caused by lattice imperfections, such as surfaces, grain boundaries, impurities, and other defect sites, is independent of temperature, and this is referred to as the residual resistivity [16]. As the material's dimensions are reduced, the residual resistivity increases because the surface-to-volume ratio increases. In addition, the high defect densities and incorporated impurities during electrodeposition may result in a higher residual resistivity compared to bulk metals.

Figure 4 shows the magnetoresistance profiles for Ni, $Co_{23}Ni_{77}$ and $Ni_{85}Fe_{15}$ nanowires measured at 10 and 300 K with an external magnetic field applied longitudinal (//) and transverse (⊥) with respect to the direction of the nanowire axis. As we expected, the overall profiles have a characteristic anisotropic magnetoresistance, which show negative longitudinal and positive transverse magnetoresistance curves, regardless of temperature. In the case of a Ni nanowire, the transverse magnetoresistance was suppressed

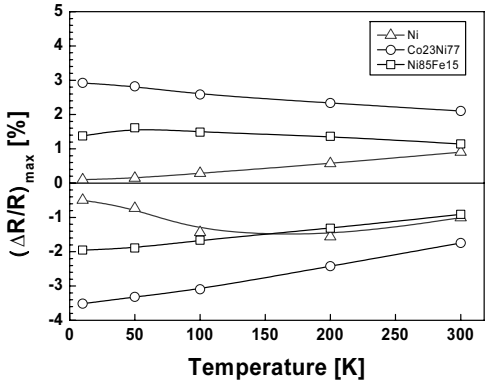

Fig. 5 Temperature dependence of maximum transverse and longitudinal magnetoresistance ratio for ferromagnetic single nanowires.

at low temperature, and this might be attributed to a change in the stress anisotropy of the Ni nanowire from a tensile stress induced by a thermal expansion mismatch between the nanowire and the Si substrate.

The maximum longitudinal and transverse magnetoresistance ratios as a function of temperature are shown in Fig. 5. The longitudinal and transverse magnetoresistance ratios are defined as

$$(\Delta R/R)_{//} = \frac{R_{//}(H) - R_{//}(H_{\max})}{R_{//}(H_{\max})} \times 100 \quad (2)$$

$$(\Delta R/R)_{\perp} = \frac{R_{\perp}(H) - R_{\perp}(H_{\max})}{R_{\perp}(H_{\max})} \times 100 \quad (3)$$

where $R_{//}(H)$ and $R_{\perp}(H)$ are the resistance in the longitudinal and transverse direction, respectively. The maximum external magnetic field, $H_{\max}$, is 10 kOe. The maximum magnetoresistance ratio for $Co_{23}Ni_{77}$ and $Ni_{85}Fe_{15}$ nanowires decreases continuously with increasing temperature, whereas that for the Ni nanowire has a maximum magnetoresistance ratio at 200 K. The anisotropic magnetoresistance ratios are 1.9, 3.8 and 2.0 % at 300 K for Ni, $Co_{23}Ni_{77}$ and $Ni_{85}Fe_{15}$ nanowires, which are much lower than bulk values [15]. These observations may result from an increased demagnetizing field in nanowires and/or scattering from impurities incorporated during electrodeposition.

In summary, the single component and alloy nanowires with 200 nm in diameter were synthesized using template-directed electrodeposition, and a single nanowire was assembled on prefabricated Au electrodes using a magnetic field assisted assembly technique. The temperature dependent magnetotransport of ferromagnetic nanowires shows anisotropic magnetoresistance. The maximum magnetoresistance of ferromagnetic nanowires was smaller than the bulk counterparts.

Acknowledgements This material is based on research sponsored by the Defense Microelectronics Activity (DMEA) under agreement number DOD/DMEA-CNN H94003-06-20604. The United States government is authorized to reproduce and distribute reprints for government purposes, not withstanding any copyright notation thereon.

References

[1] A. Wolf, D. D. Awschalom, R. A. Buhrman, J. M. Daughton, S. von Molnar, M. L. Roukes, A. Y. Chtchelkanova, and D. M. Treger, Science **294**, 1488 (2001).
[2] H. Chiriac, A. E. Moga, M. Urse, and T. A. Ovari, Sens. Actuators A **106**, 348 (2003).
[3] D. Navas, A. Asenjo, M. Jaafar, K. R. Pirota, M. Hernandez-Velez, R. Sanz, W. Lee, K. Nielsch, F. Batallan, and M. Vazquez, J. Magn. Magn. Mater. **290/291**, 191 (2005).
[4] T. Ohgai, L. Gravier, X. Hoffer, and J.-P. Ansermet, J. Appl. Electrochem. **35**, 479 (2005).
[5] G. C. Han, B. Y. Zong, P. Luo, and Y. H. Wu, J. Appl. Phys. **93**, 9202 (2003).
[6] R. Hertel, J. Appl. Phys. **90**, 5752 (2001).
[7] A. O. Adeyeye and R. L. White, J. Appl. Phys. **95**, 2025 (2004).
[8] C. M. Hangarter and N. V. Myung, Chem. Mater. **17**, 1320 (2005).
[9] B. Y. Yoo, Y. Rheem, W. P. Beyermann, and N. V. Myung, Nanotechnology **17**, 2512 (2006).
[10] C. M. Hangarter, Y. Rheem, B. Y. Yoo, E. H. Yang, and N. V. Myung, Nanotechnology **18**, 205305 (2007).
[11] Y. Rheem, B. Y. Yoo, W. P. Beyermann, and N. V. Myung, Nanotechnology **18**, 15202 (2007).
[12] Y. Rheem, B. Y. Yoo, W. P. Beyermann, and N. V. Myung, Nanotechnology **18**, 125204 (2007).
[13] Y. Rheem, B. Y. Yoo, W. P. Beyermann, and N. V. Myung, Nanotechonlogy (2007), submitted.
[14] N. V. Myung, K. Nobe, J. Electrochem. Soc. **148**, C136 (2001).
[15] R. M. Bozorth, Ferromagnetism (John Wiley & Sons, Inc., New Jersey, 1951).
[16] A. Fert and I. A. Campbell, J. Phys. F **6**, 849 (1976).

